AJNR

Surveillance of Unruptured Intracranial Saccular Aneurysms Using Noncontrast 3D-Black-Blood MRI: Comparison of 3D-TOF and Contrast-Enhanced MRA with 3D-DSA

C. Zhu, X. Wang, L. Eisenmenger, B. Tian, Q. Liu, A.J. Degnan, C. Hess, D. Saloner and J. Lu

AJNR Am J Neuroradiol 2019, 40 (6) 960-966
doi: https://doi.org/10.3174/ajnr.A6080
http://www.ajnr.org/content/40/6/960

Surveillance of Unruptured Intracranial Saccular Aneurysms Using Noncontrast 3D-Black-Blood MRI: Comparison of 3D-TOF and Contrast-Enhanced MRA with 3D-DSA

C. Zhu, X. Wang, L. Eisenmenger, B. Tian, Q. Liu, A.J. Degnan, C. Hess, D. Saloner, and J. Lu

ABSTRACT

BACKGROUND AND PURPOSE: Patients with unruptured intracranial aneurysms routinely undergo surveillance imaging to monitor growth. Angiography is the criterion standard for aneurysm diagnosis, but it is invasive. This study aimed to evaluate the accuracy and reproducibility of a 3D noncontrast black-blood MR imaging technique for unruptured intracranial aneurysm measurement in comparison with 3D-TOF and contrast-enhanced MRA, using 3D rotational angiography as a reference standard.

MATERIALS AND METHODS: Sixty-four patients (57.3 ± 10.9 years of age, 41 women) with 68 saccular unruptured intracranial aneurysms were recruited. Patients underwent 3T MR imaging with 3D-TOF-MRA, 3D black-blood MR imaging, and contrast-enhanced MRA, and they underwent 3D rotational angiography within 2 weeks. The neck, width, and height of the unruptured intracranial aneurysms were measured by 2 radiologists independently on 3D rotational angiography and 3 MR imaging sequences. The accuracy and reproducibility were evaluated by Bland-Altman plots, the coefficient of variance, and the intraclass correlation coefficient.

RESULTS: 3D black-blood MR imaging demonstrates the best agreement with DSA, with the smallest limits of agreement and measurement error (coefficients of variance range, 5.87%–7.04%). 3D-TOF-MRA had the largest limits of agreement and measurement error (coefficients of variance range, 12.73%–15.78%). The average coefficient of variance was 6.26% for 3D black-blood MR imaging, 7.03% for contrast-enhanced MRA, and 15.54% for TOF-MRA. No bias was found among 3 MR imaging sequences compared with 3D rotational angiography. All 3 MR imaging sequences had excellent interreader agreement (intraclass correlation coefficient, >0.95). 3D black-blood MR imaging performed the best for patients with intraluminal thrombus ($n = 10$).

CONCLUSIONS: 3D black-blood MR imaging achieves better accuracy for aneurysm size measurements compared with 3D-TOF, using 3D rotational angiography as a criterion standard. This noncontrast technique is promising for surveillance of unruptured intracranial aneurysms.

ABBREVIATIONS: BB = black-blood; CE = contrast-enhanced; CV = coefficient of variance; 3DRA = 3D rotational angiography; IA = intracranial aneurysm; ICC = intraclass correlation coefficient; LOA = limit of agreement; SPACE = spatial and chemical-shift encoded excitation; UIA = unruptured intracranial aneurysm

Intracranial aneurysms (IAs) are common, with approximately 3% of adults having an unruptured IA (UIA).[1] UIAs are associated with morbidity and mortality due to the risk of rupture and the resultant subarachnoid hemorrhage.[2] Of patients surviving ruptured IAs, 30% will experience high morbidity due to associated intraparenchymal hemorrhage from late-onset complications such as vasospasm leading to cerebral infarction. Only approximately one-third of patients with subarachnoid hemorrhage related to IA rupture will fully return to their prior jobs,[3,4] but diagnosis of IAs before rupture may improve patient outcomes.[5]

Clinical management of UIAs is based largely on aneurysm size and other features such as location, shape, and sac-to-neck

Received February 22, 2019; accepted after revision April 15.

From the Department of Radiology and Biomedical Imaging (C.Z., L.E., C.H., D.S.), University of California, San Francisco, San Francisco, California; Department of Radiology (X.W., B.T., Q.L., J.L.), Changhai Hospital, Shanghai, China; Department of Radiology (X.W.), General Hospital of Northern Military Command, Liaoning, China; and Department of Radiology (A.J.D.), Children's Hospital of Philadelphia, Philadelphia, Pennsylvania.

Chengcheng Zhu and Xinrui Wang contributed equally to this work.

This work was supported by the National Natural Science Foundation of China (No. 81670396, No. 31470910), and the National Institutes of Health, grant K99HL136883.

The sponsoring organizations had no involvement in the study design, data collection, data analysis, data interpretation, writing of the article, or the decision to submit for publication.

Please address correspondence to Jianping Lu, MD, Department of Radiology, Changhai Hospital, Shanghai, China; e-mail: cjr.lujianping@vip.163.com

Indicates open access to non-subscribers at www.ajnr.org
Indicates article with supplemental on-line table.
Indicates article with supplemental on-line photo.
http://dx.doi.org/10.3174/ajnr.A6080

ratio, with saccular aneurysms being the most common type.[6-9] Because intervention-associated risks may exceed the low rupture rates for smaller UIAs,[5] most of those small aneurysms are followed with surveillance instead of immediate treatment. In addition, more incidental UIAs have been found on widely used noninvasive imaging techniques. Usually, incidental UIAs that are regular in shape and <7 mm are followed up to assess changes with time that may modify clinical decision-making,[10] but how to best diagnose and monitor UIAs remains uncertain.

Although 3D rotational angiography (3DRA) is the criterion standard for diagnosing IAs as well as evaluating IA morphology measurements,[11] both MR imaging and CTA have become increasingly important in evaluating UIAs. This change is largely because both MR imaging and CTA are less invasive than 3DRA, reducing the risks of IA screening and monitoring of known UIAs.[12-14] However, unlike MR imaging, both 3DRA and CTA expose patients to ionizing radiation and iodinated contrast media. MR imaging is an option that removes the uncertain risks of repeat radiation and contrast media exposure.

Vascular MR imaging has substantially improved with the development of techniques enabling the diagnosis, visualization, and assessment of intracranial aneurysms with high accuracy.[15] Numerous studies have assessed the value of both flow-based (TOF) and contrast-enhanced (CE) MRA techniques.[5] Fewer studies have evaluated 3D noncontrast black-blood (BB) MR imaging in aneurysm characterization, though early data have shown promise[15] with the use of high-isotropic resolution (up to 0.5 mm) to visualize the aneurysm geometry and wall.[16] 3D-BB MR imaging, however, has not been validated against 3DRA for aneurysm size measurements or compared with other clinical MRA techniques. This study aimed to compare black-blood MR imaging with 3D-TOF/CE-MRA for aneurysm size measurements using 3DRA as a reference standard. We hypothesized that 3D noncontrast BB MR imaging can be used to measure aneurysm size accurately.

MATERIALS AND METHODS

Study Population

This study was approved by the institutional review board of Changhai Hospital. Informed consent was obtained from all patients. A total of 69 consecutive patients with confirmed saccular IAs were recruited between January 2016 and March 2018. All patients underwent 3T MR imaging and 3DRA within 2 weeks.

Imaging Protocol

MR Imaging. MR imaging was performed on a 3T whole-body MR imaging system (Magnetom Skyra; Siemens, Erlangen, Germany) using a 20-channel head coil. 3D-TOF-MRA, 3D-BB MR imaging, and CE-MRA were performed successively. The unenhanced 3D-TOF-MRA was performed with TR = 21 ms, TE = 3.4 ms, flip angle = 20°, FOV = 180 × 200 mm^2, matrix = 330 × 384, in-plane resolution = 0.5 × 0.5 mm^2, slice thickness = 0.7 mm, 144 slices, and total acquisition time of 4 minutes 56 seconds. The 3D-BB MR imaging (spatial and chemical-shift encoded excitation [SPACE]) was performed with TR = 900 ms, TE = 5.6 ms, FOV = 160 × 160, matrix = 320 × 320, slice thickness = 0.5 mm, echo-train length = 60, 280 slices, and total acquisition time of 8 minutes 16 seconds. CE-MRA was then performed at the first pass of intravenous injection of Gd-DTPA at a dose of 0.1 mmol/kg, using a FLASH 3D spoiled gradient-echo sequence with TR = 3.66 ms, TE = 1.44 ms, FOV = 182 × 224 mm^2, flip angle = 20°, matrix = 320 × 320, in plane resolution = 0.6 × 0.7 mm^2, slice thickness = 0.7 mm, 120 slices, and total acquisition time of 1 minute 24 seconds.

3DRA. 3DRA was performed on the Artis zee Biplane angiographic system (VC14; Siemens). A 5-second DSA acquisition protocol was performed with contrast injection at a rate of 3 mL/s of Ultravist (iopromide; Bayer HealthCare, Berlin, Germany). During the 5-second acquisition after a delay of 1 second, a 200° rotation of the C-arm was performed to obtain 133 frames. The parameters were as follows: FOV = 320 × 320 mm^2, matrix = 1024 × 1024.

Image Analysis

Image analysis was performed independently by 2 radiologists (X.W. and B.T. with 5 and 9 years of experience) who were blinded to patients' clinical data. All measurements were conducted on the postprocessing workstation (syngo X Workspace; Siemens). Measurement of 3DRA was performed on volume-rendered reconstruction, and measurements of TOF-MRA and CE-MRA were performed on MIP reconstructions. The MIP images were imported to the workstation, and the image viewer automatically set a default window/level for the best display. In addition, 2 observers were also allowed to adjust the window/level and projection angles to best display the aneurysm and the parent vessel. Measurement of 3D-BB MR imaging was performed on MPR images.

For each IA, we measured the following parameters: 1) height: the maximum distance from the neck center to the dome of the aneurysm; 2) width: the longest diameter of an aneurysm perpendicular to the height; and 3) neck: the minimum width of the aneurysm at its junction with the parent vessel (Fig 1). Measurements were performed by the 2 readers (X.W. and B.T.) separately, with an interval of 2 weeks between different modalities. One reader performed the second measurement (X.W.) 2 weeks later using the same method to evaluate the intrareader variability. All these measurements were performed only for the luminal geometry, for which DSA could be used as a reference standard. If the aneurysms had intraluminal thrombus, the images were evaluated separately for the true aneurysm geometry.

Statistical Analysis

Normality assumptions were assessed using the Shapiro-Wilk test. Continuous variables were expressed as either mean ± SD or median (interquartile range). Categoric variables were summarized by count (percentage). Comparisons of aneurysm height, width, and neck diameter among different imaging modalities were analyzed using the Kruskal-Wallis test. Measurement differences between MR imaging modalities and DSA as well as intra- and interreader variabilities were assessed using the Bland-Altman analysis. Bias was assessed as the mean of the pair differences, and the 95% limits of agreement (LOA) were defined as bias ± 1.96 × SD. Measurement error was quantified by the coefficient of variance (CV = SD / mean × 100%). Agreement between

measurements was summarized by the intraclass correlation coefficient (ICC) with a 2-way mixed model. An ICC value >0.80 indicated excellent agreement. On the basis of the measurement errors of each MR imaging sequence, the sample sizes needed to detect 5%, 10%, and 20% changes in aneurysm size growth in longitudinal studies were calculated by using 0.9 power and .05 significance as described in a previous publication.[17] Statistical analyses were performed using SPSS, Version 24.0 (IBM, Armonk, New York) and MedCalc for Windows, Version 9.4.2.0 (MedCalc Software, Mariakerke, Belgium).

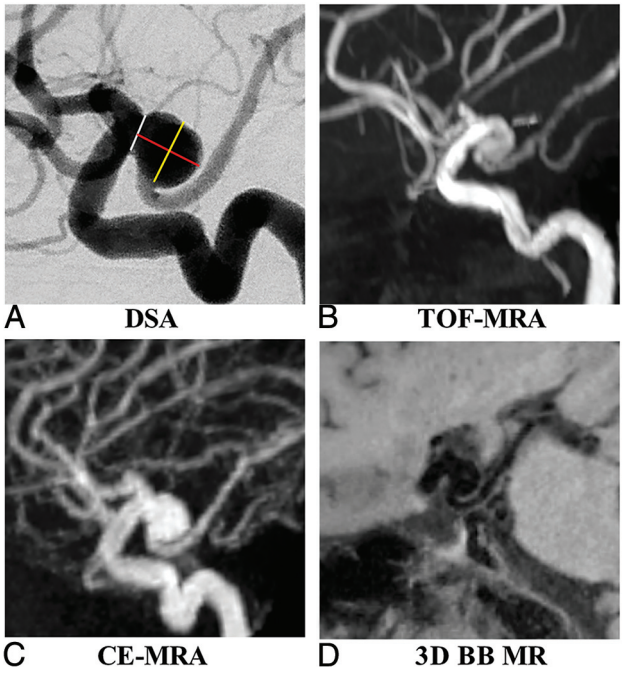

FIG 1. A 61-year-old woman with a right posterior communicating artery aneurysm on DSA (*A*), TOF-MRA (*B*), CE-MRA (*C*), and 3D-BB MR imaging (*D*). Aneurysm height (*red line*), width (*yellow line*), and neck (*white line*) measurements are demonstrated in *A*.

RESULTS

Of the 69 recruited patients, 5 were excluded for the following reasons: 1) an interval of >2 weeks between MR imaging and DSA ($n = 2$); 2) a ruptured aneurysm ($n = 1$); and 3) insufficient image quality due to motion artifacts on 3D-BB MR imaging ($n = 2$). The remaining 64 patients (57.3 ± 10.9 years of age, 41 women) with 68 saccular UIAs were included. UIAs were located in the internal carotid artery ($n = 32$), middle cerebral artery ($n = 12$), anterior communicating artery ($n = 10$), posterior communicating artery and posterior cerebral artery ($n = 8$), and vertebral-basilar artery ($n = 6$). The average interval between MR imaging and DSA was 2.2 ± 1.6 days (range, 1–9 days). Mild flow artifacts were observed in 3 UIAs with aneurysm diameters of >15 mm on 3D-BB MR imaging. These artifacts did not affect the measurement accuracy.

Agreement between MR Imaging Sequences and DSA

As shown in Table 1, there was no significant difference in aneurysm height, width, and neck diameter among TOF/CE-MRA, 3D-BB MR imaging, and DSA ($P > .05$). Agreement of the quantitative measurements between MR imaging modalities and DSA is summarized in Table 2. Bland-Altman plots for each measurement are shown in Fig 2 and the On-line Figure. Measurements between MR imaging modalities and DSA showed excellent agreement with ICCs of >0.96. Measurement on TOF-MRA showed the largest variance (overall CV, 15.54%) and higher LOA compared with measurements on CE-MRA (overall CV, 7.03%) and 3D-BB MR imaging (overall CV, 6.26%). Based on the measurement errors of each MR image, the calculated sample sizes in future longitudinal studies to detect 5%, 10%, and 20% change in aneurysm growth are shown in Table 3. Compared with 3D-TOF, the use of CE-MRA or 3D-BB MR imaging reduces the sample size

Table 1: Comparison of aneurysm height, width, and neck measurements among MR and DSA imaging modalities[a]

	TOF-MRA	CE-MRA	3D-BB MRI	3DRA	*P* Value
Height (mm)	7.7 (5.5–11.1)	8.0 (6.0–12.8)	7.8 (5.4–12.6)	7.7 (5.5–12.6)	.918
Width (mm)	7.5 (5.8–11.5)	8.4 (5.8–14.0)	7.8 (5.5–13.9)	8.1 (5.9–13.3)	.957
Neck (mm)	6.8 (5.3–10.4)	6.7 (5.2–10.6)	7.0 (4.8–10.2)	6.9 (4.6–9.8)	.774

[a] Data are median (interquartile range).

Table 2: Comparison of MRI techniques with DSA for aneurysm measurements

	Mean (mm)	SD	CV (100%)	Bias	LOA	ICC
Height						
TOF-MRA	9.21	1.50	15.43	−0.55	(−3.49–2.39)	0.96 (0.93–0.98)
CE-MRA	9.90	0.62	6.32	0.14	(−1.08–1.36)	0.98 (0.97–0.99)
3D-BB MRI	9.73	0.59	6.04	−0.03	(−1.19–1.13)	0.99 (0.99–0.99)
Width						
TOF-MRA	9.53	1.56	15.78	−0.33	(−2.73–3.39)	0.96 (0.94–0.97)
CE-MRA	10.12	0.61	6.18	0.26	(−0.94–1.46)	0.99 (0.98–0.99)
3D-BB MRI	9.96	0.58	5.87	0.10	(−1.04–1.24)	0.99 (0.99–0.99)
Neck						
TOF-MRA	8.00	0.98	12.73	0.31	(−1.61–2.23)	0.96 (0.93–0.98)
CE-MRA	8.08	0.68	8.81	0.39	(−0.94–1.72)	0.97 (0.95–0.99)
3D-BB MRI	7.71	0.54	7.04	0.02	(−1.04–1.08)	0.98 (0.98–0.99)
Overall						
TOF-MRA	8.91	1.41	15.54	−0.19	(−2.95–2.57)	0.96 (0.95–0.97)
CE-MRA	9.37	0.64	7.03	0.26	(−0.99–1.51)	0.98 (0.98–0.99)
3D-BB MRI	9.14	0.57	6.26	0.03	(−1.08–1.15)	0.99 (0.99–0.99)

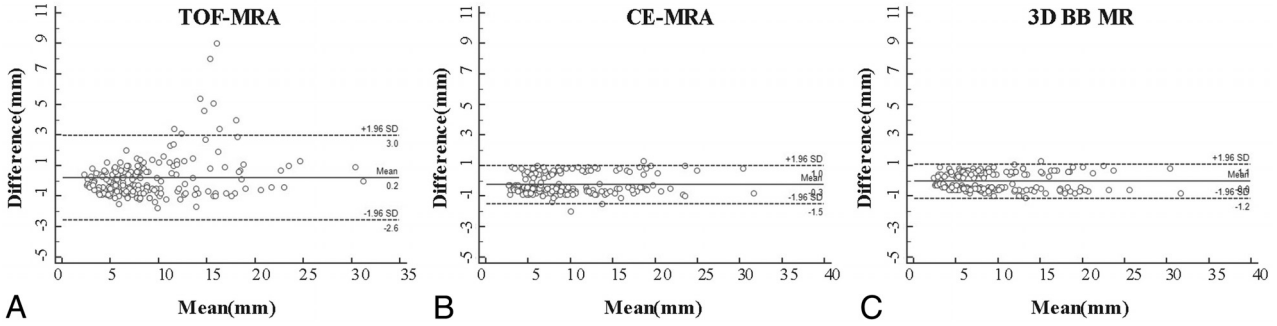

FIG 2. Bland-Altman plots of aneurysm measurements of TOF-MRA (*A*), CE-MRA (*B*), and 3D-BB MR imaging (*C*) versus 3DRA as the reference standard. *Solid horizontal lines* define the reference standard, and *upper and lower dashed lines* define the LOA.

Table 3: Sample size calculation using different MRI sequences to detect aneurysm growth

Aneurysm Growth	TOF-MRA (CV = 15.54%)	CE-MRA (CV = 7.03%)	SPACE (CV = 6.26%)
5%	406	84	66
10%	102	21	17
20%	26	6	5

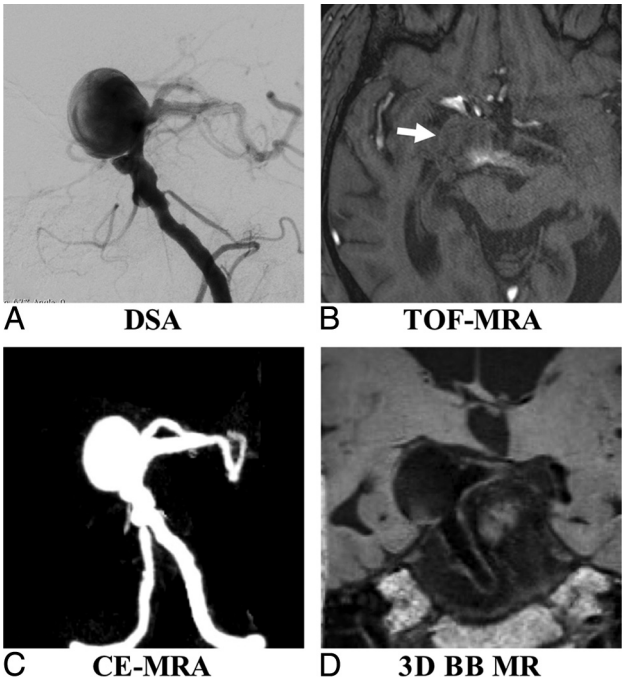

FIG 3. A 53-year-old man with multiple basilar artery aneurysms on DSA (*A*). The aneurysm shows isointensity on TOF-MRA (*B*) because of the slow flow (*arrow*). The aneurysm sac and neck were integrally visualized on CE-MRA (*C*) and 3D-BB MR imaging (*D*).

by 79% and 84%, respectively. Comparisons of MR imaging modalities with DSA for aneurysm measurements by locations are summarized in On-line Table. The measurement errors did not vary significantly across locations.

Sample patient images are shown in Figs 3 and 4. Figure 3 shows that TOF is limited as a means of displaying the aneurysm geometry due to severe flow artifacts, while DSA, CE-MRA, and SPACE characterize the geometry nicely. Figure 4 shows an aneurysm with intraluminal thrombus. 3D-BB MR imaging can clearly show the entire aneurysm structure including both the lumen and the thrombus.

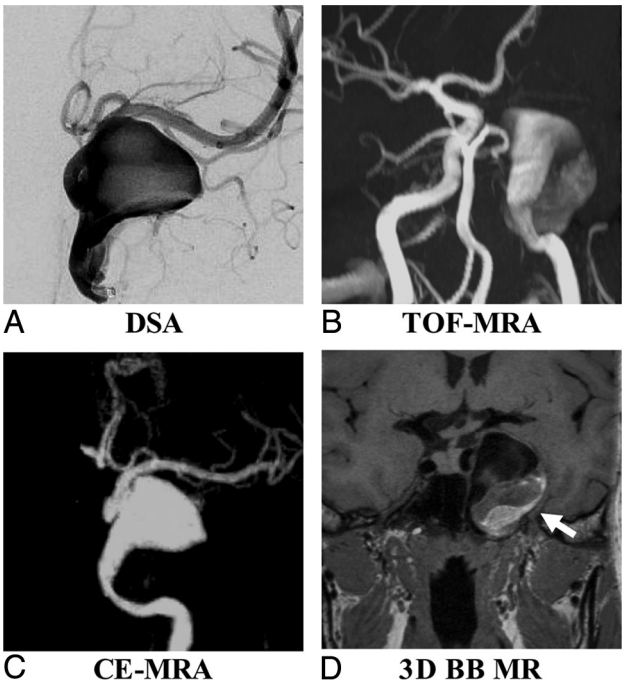

FIG 4. A 63-year-old woman with a right middle cerebral artery aneurysm on DSA (*A*). 3D-BB SPACE (*D*) can clearly visualize the sac and intraluminal thrombus of the aneurysm, which is superior to DSA (*A*), TOF-MRA (*B*), and CE-MRA (*C*).

Intra- and Interreader Agreement

Intra- and interreader agreement is shown in Table 4. There were no significant mean differences between readers ($P > .05$). The overall intra- and interreader measurements showed excellent agreement, with ICCs of >0.97.

Aneurysms with Intraluminal Thrombus

Ten aneurysms were found with intraluminal thrombus: 3 aneurysms located in the middle cerebral artery, 2 located in the internal carotid artery, 2 located in the anterior communicating artery, 2 located in the posterior communicating artery, and 1 located in the basilar artery. Aneurysm sizes ranged from 8.0 to 28.2 mm. 3D-BB MR imaging gave the best evaluation of aneurysm dimensions, with clear delimitation of both the lumen and thrombus (Fig 3). The median thickness of the intraluminal thrombus was 2.8 mm (IQR, 0.8–4.4 mm).

Table 4: Intra- and interreader agreement for aneurysm measurements

	CV (100%)	Bias	LOA	ICC
Intrareader agreement				
Height				
TOF-MRA	7.02	0.19	(−0.87–1.25)	0.99 (0.98–0.99)
CE-MRA	6.71	0.14	(−1.09–1.37)	0.99 (0.98–0.99)
3D-BB MRI	6.37	−0.08	(−1.18–1.02)	0.99 (0.98–0.99)
3DRA	6.87	0.14	(−1.04–1.32)	0.99 (0.98–0.99)
Width				
TOF-MRA	6.94	0.06	(−0.99–1.12)	0.99 (0.98–0.99)
CE-MRA	6.45	0.10	(−1.13–1.33)	0.99 (0.98–0.99)
3D-BB MRI	6.31	0.18	(−0.92–1.28)	0.99 (0.98–0.99)
3DRA	6.25	0.11	(−1.00–1.23)	0.99 (0.98–0.99)
Neck				
TOF-MRA	7.29	0.18	(−1.04–1.39)	0.98 (0.98–0.99)
CE-MRA	7.05	0.13	(−0.93–1.19)	0.99 (0.98–0.99)
3D-BB MRI	6.72	0.14	(−0.90–1.18)	0.99 (0.98–0.99)
3DRA	6.98	−0.08	(−1.17–1.02)	0.99 (0.98–0.99)
Overall				
TOF-MRA	7.08	0.14	(−0.78–1.06)	0.99 (0.98–0.99)
CE-MRA	6.78	0.12	(−1.06–1.30)	0.99 (0.98–0.99)
3D-BB MRI	6.51	0.08	(−0.96–1.12)	0.99 (0.98–0.99)
3DRA	6.75	0.06	(−1.04–1.16)	0.99 (0.98–0.99)
Interreader agreement				
Height				
TOF-MRA	8.12	0.02	(−1.45–1.49)	0.98 (0.98–0.99)
CE-MRA	8.19	0.23	(−1.33–1.80)	0.98 (0.98–0.99)
3D-BB MRI	8.03	0.03	(−1.50–1.56)	0.98 (0.98–0.99)
3DRA	7.87	−0.07	(−1.58–1.44)	0.98 (0.98–0.99)
Width				
TOF-MRA	8.03	−0.03	(−1.50–1.44)	0.98 (0.98–0.99)
CE-MRA	7.55	0.17	(−1.30–1.64)	0.99 (0.98–0.99)
3D-BB MRI	8.37	0.03	(−1.61–1.67)	0.98 (0.98–0.99)
3DRA	7.15	−0.13	(−1.54–1.28)	0.99 (0.98–0.99)
Neck				
TOF-MRA	8.96	0.18	(−0.74–1.10)	0.97 (0.95–0.98)
CE-MRA	8.81	0.07	−0.81–1.07)	0.98 (0.97–0.99)
3D-BB MRI	8.95	0.14	(−0.72–1.00)	0.98 (0.97–0.99)
3DRA	8.82	0.10	(−0.82–0.98)	0.98 (0.97–0.99)
Overall				
TOF-MRA	8.44	0.06	(−0.78–1.06)	0.98 (0.98–0.99)
CE-MRA	8.16	0.16	(−0.74–0.98)	0.98 (0.98–0.99)
3D-BB MRI	8.43	0.07	(−0.63–0.93)	0.98 (0.98–0.99)
3DRA	8.15	−0.03	(−0.72–1.00)	0.98 (0.98–0.99)

DISCUSSION

In this study, measurements obtained on 3D-BB MR imaging were in close agreement with 3DRA measurements and had a better accuracy than 3D-TOF with less than half the TOF measurement error. The sample size needed to measure aneurysm size change in longitudinal studies would be reduced by 84% using 3D-BB MR imaging compared with using 3D-TOF. Our results support the use of noncontrast 3D-BB MR imaging for intracranial aneurysm surveillance. Despite previous studies evaluating the use of BB MR imaging sequences in the characterization of IAs, this is the first study to validate 3D-BB MR imaging against the criterion standard 3DRA for aneurysm morphology measurements. In addition, this is the first study to compare 3D-BB MR imaging with 3D-TOF and CE-MRA for IA measurement accuracy.

Although 3DRA remains the criterion standard in aneurysm evaluation and treatment planning with high spatial resolution and excellent hemodynamic temporal resolution,[11] DSA is invasive with procedural risks such as arterial dissection, hematomas, stroke, and even death that are more important than the small theoretic risks of radiation and contrast exposure.[18] Alternatively, CTA is a fast, noninvasive imaging test that is often used in first-line aneurysm assessment. CTA has widespread availability and has been shown to be of benefit in not only aneurysm detection[19-23] but also presurgical planning.[24] Despite the advantages of CTA, like DSA, CTA uses radiation and iodinated contrast, reducing its adoption in UIA screening and monitoring.[12] MR imaging does not have these issues.[25] Other disadvantages of CTA include the fact that despite the development of improved techniques in the region of the skull base,[26,27] MR imaging lacks the attenuation and streak artifacts occasionally encountered in CTA.[28] MR imaging can play a major role in UIA detection, monitoring, and treatment planning.[29]

3D-TOF and CE-MRA are commonly used methods for UIA evaluation. 3D-TOF-MRA is a popular method because it does not require a contrast agent[10,30,31]; however, it has flow artifacts and can confuse T1-weighted hyperintense thrombus within an aneurysm with flow-related enhancement.[32,33] Bright thrombus can mimic flowing lumen, and isointense thrombus is difficult to distinguish from surrounding brain tissue.[15] TOF-MRA can also make detection of IAs difficult in the setting of T1 hyperintense intraparenchymal or subarachnoid hemorrhage.[34-36] Our study observed that while still similar to 3DRA, 3D-TOF-MRA had the least accuracy of the MR imaging–based methods tested, in accordance with previous literature.

CE-MRA is an accurate method for UIA evaluation because it is not flow-dependent.[37] CE-MRA was shown to be superior to 3D-TOF-MRA for assessment of sac shape, visualizing an aneurysm neck, calculating of the sac/neck ratio, and identifying branches originating from the sac and/or neck,[5] especially for large aneurysms (>13 mm), when flow artifacts were commonly present. Despite these advantages of CE-MRA, its limitations include the use of gadolinium-based contrast media, dependence on timing of contrast administration that may lead to venous contamination, and radiofrequency power deposition at high field strengths.[38] Recent concerns regarding gadolinium deposition in the brain parenchyma, while uncertain and controversial, call into question its widespread use in repeat imaging for surveillance.[39]

When we compared it with other imaging modalities, 3D-BB

MR imaging has clear advantages. First, it is an accurate method for UIA measurements as evidenced in the superior agreement of this study with DSA, which was comparable with CE-MRA. Although our CE-MRA protocol had better resolution (around 0.7 mm isotropic) than most routine clinical protocols (0.9–1.1 mm),[5] 3D-BB MR imaging had an even higher resolution (0.5 mm isotropic), which may explain its slightly improved accuracy. 3D-BB MR imaging has also been used for intracranial stenosis quantification[11] and extracranial carotid plaque imaging[40] in studies showing excellent agreement with DSA. Our study extends these observations in showing that 3D-BB MR imaging provides accurate assessment of aneurysms. The high accuracy of 3D-BB MR imaging is favorable for future longitudinal studies, which can reduce sample size more significantly than with 3D-TOF and reduce the cost of the clinical trial. Accurate quantification of aneurysm growth is important because fast-growing aneurysms have a much higher risk of rupture.[41,42]

Second, as a noncontrast acquisition, 3D-BB MR imaging is ideal for repeat, routine surveillance of UIAs compared with contrast techniques including CE-MRA and CTA. It can also be repeated if the first acquisition fails due to patient motion or other issues. Third, 3D-BB SPACE is insensitive to flow artifacts, which is superior to 3D-TOF (Figs 3 and 4). The 3D fast-spin-echo BB sequence is inherently blood-suppressed.[43] Although in large aneurysms, flow artifacts can still occur, several additional techniques, including improved motion-sensitized driven-equilibrium[44] and delay alternating with nutation for tailored excitation (DANTE)[45] may be used to optimize blood suppression. Previous work comparing 3D-TOF and BB techniques showed significant advantages to BB imaging in cases of large aneurysms or slow blood flow.[36,46] In 1 study, the authors found 3 patients in whom the aneurysm was not demonstrated on 3D-TOF due to the presence of local hematoma, but by performing a BB sequence, they found that all of the IAs were subsequently identified without the need for contrast.[15]

Last, 3D-BB MR imaging can also visualize intraluminal thrombus and the vessel wall, which is a unique advantage in comparison with angiographic methods. Because vessel wall features and postcontrast enhancement have been studied as potential markers of aneurysm rupture,[25,47] this ability could become increasingly important in aneurysm characterization and monitoring.

Limitations

There are some limitations to this study. First, we evaluated only saccular aneurysms with fusiform aneurysms excluded. Second, our current 3D-BB MR imaging sequence has a scan time of approximately 9 minutes, greater than the time it takes for either CE-MRA (2–3 minutes) or TOF (~5 minutes). It is possible that a lower resolution (0.6–0.7 mm isotropic) can achieve sufficient accuracy with a significantly reduced scan time. Advanced acceleration techniques, including compressed sensing, may potentially reduce the scan time significantly with similar image quality.[48] Future studies are needed to determine the minimum spatial resolution necessary and apply new acceleration techniques clinically. Third, the image-reconstruction methods were not the same across imaging modalities. We used the reconstruction methods that were conventionally used in clinical routine,[15,49,50] and also note that the influence of reconstruction methods for aneurysm measurements has been rarely studied. However, we believe the differences caused by reconstruction methods were much less than the differences caused by imaging techniques, as shown in our data.

Despite these limitations, we believe that they are offset by the improved IA measurements compared with the other MR imaging techniques as well as the ability of 3D-BB MR imaging to characterize the vessel wall without the use of gadolinium-based contrast, supporting the use of noncontrast BB MR imaging to replace CE-MRA in monitoring IAs.

CONCLUSIONS

3D-BB MR imaging achieves superior accuracy for intracranial aneurysm size measurements over 3D-TOF using 3DRA as the criterion standard, though all MR imaging measurements did not significantly differ from those with 3DRA. This noncontrast technique is promising for clinical surveillance of patients with unruptured intracranial aneurysms.

Disclosures: Christopher Hess—*UNRELATED: Expert Testimony*: various medicolegal firms; *Grants/Grants Pending*: National Institutes of Health*; *Travel/Accommodations/Meeting Expenses Unrelated to Activities Listed*: Korean Society of Radiology, MRI Garmisch Symposium, *Comments*: Korean Society of Radiology; travel costs to lecture and participate in Korean Congress of Radiology 2018 and 18th MRI International MRI Symposium Garmisch-Partenkirchen. *Money paid to individual.

REFERENCES

1. Wiebers DO, Whisnant JP, Huston J 3rd, et al; International Study of Unruptured Intracranial Aneurysms Investigators. **Unruptured intracranial aneurysms: natural history, clinical outcome, and risks of surgical and endovascular treatment.** *Lancet* 2003;362:103–10 CrossRef Medline
2. Fogelholm R, Hernesniemi J, Vapalahti M. **Impact of early surgery on outcome after aneurysmal subarachnoid hemorrhage: a population-based study.** *Stroke* 1993;24:1649–54 CrossRef Medline
3. Passier PE, Visser-Meily JM, Rinkel GJ, et al. **Life satisfaction and return to work after aneurysmal subarachnoid hemorrhage.** *J Stroke Cerebrovasc Dis* 2011;20:324–29 CrossRef Medline
4. Rinkel GJ, Algra A. **Long-term outcomes of patients with aneurysmal subarachnoid haemorrhage.** *Lancet Neurol* 2011;10:349–56 CrossRef Medline
5. Cirillo M, Scomazzoni F, Cirillo L, et al. **Comparison of 3D TOF-MRA and 3D CE-MRA at 3T for imaging of intracranial aneurysms.** *Eur J Radiol* 2013;82:e853–59 CrossRef Medline
6. Komotar RJ, Starke RM, Connolly ES. **The natural course of unruptured cerebral aneurysms.** *Neurosurgery* 2012;71:N7–9 CrossRef Medline
7. Backes D, Vergouwen MD, Tiel Groenestege AT, et al. **PHASES score for prediction of intracranial aneurysm growth.** *Stroke* 2015;46:1221–26 CrossRef Medline
8. Gibbs GF, Huston J 3rd, Bernstein MA, et al. **Improved image quality of intracranial aneurysms: 3.0-T versus 1.5-T time-of-flight MR angiography.** *AJNR Am J Neuroradiol* 2004;25:84–87 Medline
9. Nael K, Villablanca JP, Mossaz L, et al. **3T contrast-enhanced MR angiography in evaluation of suspected intracranial aneurysm: comparison with MDCT angiography.** *AJR Am J Roentgenol* 2008;190:389–95 CrossRef Medline
10. Anzalone N, Scomazzoni F, Cirillo M, et al. **Follow-up of coiled cerebral aneurysms at 3T: comparison of 3D time-of-flight MR angiography and contrast-enhanced MR angiography.** *AJNR Am J Neuroradiol* 2008;29:1530–36 CrossRef Medline
11. Park JE, Jung SC, Lee SH, et al. **Comparison of 3D magnetic reso-**

nance imaging and digital subtraction angiography for intracranial artery stenosis. *Eur Radiol* 2017;27:4737–46 CrossRef Medline
12. van der Schaaf IC, Velthuis BK, Wermer MJ, et al; ASTRA Study Group. **New detected aneurysms on follow-up screening in patients with previously clipped intracranial aneurysms: comparison with DSA or CTA at the time of SAH.** *Stroke* 2005;36:1753–58 CrossRef Medline
13. Wermer MJ, Buskens E, van der Schaaf IC, et al. **Yield of screening for new aneurysms after treatment for subarachnoid hemorrhage.** *Neurology* 2004;62:369–75 CrossRef Medline
14. Wermer MJ, van der Schaaf IC, Velthuis BK, et al. **Yield of short-term follow-up CT/MR angiography for small aneurysms detected at screening.** *Stroke* 2006;37:414–18 CrossRef Medline
15. Stivaros SM, Harris JN, Adams W, et al. **Does black blood MRA have a role in the assessment of intracerebral aneurysms?** *Eur Radiol* 2009;19:184–92 CrossRef Medline
16. Zhu C, Haraldsson H, Tian B, et al. **High resolution imaging of the intracranial vessel wall at 3 and 7 T using 3D fast spin echo MRI.** *MAGMA* 2016;29:559–70 CrossRef Medline
17. Zhang X, Zhu C, Peng W, et al. **Scan-rescan reproducibility of high resolution magnetic resonance imaging of atherosclerotic plaque in the middle cerebral artery.** *PLoS One* 2015;10:e0134913 CrossRef Medline
18. Kaufmann TJ, Huston J 3rd, Mandrekar JN, et al. **Complications of diagnostic cerebral angiography: evaluation of 19,826 consecutive patients.** *Radiology* 2007;243:812–19 CrossRef Medline
19. Tipper G, U-King-Im JM, Price SJ, et al. **Detection and evaluation of intracranial aneurysms with 16-row multislice CT angiography.** *Clin Radiol* 2005;60:565–72 CrossRef Medline
20. Chen CY, Hsieh SC, Choi WM, et al. **Computed tomography angiography in detection and characterization of ruptured anterior cerebral artery aneurysms at uncommon location for emergent surgical clipping.** *Clin Imaging* 2006;30:87–93 CrossRef Medline
21. Carstairs SD, Tanen DA, Duncan TD, et al. **Computed tomographic angiography for the evaluation of aneurysmal subarachnoid hemorrhage.** *Acad Emerg Med* 2006;13:486–92 CrossRef Medline
22. Uysal E, Yanbuloğlu B, Ertürk M, et al. **Spiral CT angiography in diagnosis of cerebral aneurysms of cases with acute subarachnoid hemorrhage.** *Diagn Interv Radiol* 2005;11:77–82 Medline
23. Goddard AJ, Tan G, Becker J. **Computed tomography angiography for the detection and characterization of intra-cranial aneurysms: current status.** *Clin Radiol* 2005;60:1221–36 CrossRef Medline
24. Suzuki Y, Nakajima M, Ikeda H, et al. **Preoperative evaluation of the venous system for potential interference in the clipping of cerebral aneurysm.** *Surg Neurol* 2004;61:357–64; discussion 364 CrossRef Medline
25. Edjlali M, Gentric JC, Régent-Rodriguez C, et al. **Does aneurysmal wall enhancement on vessel wall MRI help to distinguish stable from unstable intracranial aneurysms?** *Stroke* 2014;45:3704–06 CrossRef Medline
26. Tomandl BF, Hammen T, Klotz E, et al. **Bone-subtraction CT angiography for the evaluation of intracranial aneurysms.** *AJNR Am J Neuroradiol* 2006;27:55–59 Medline
27. Sakamoto S, Kiura Y, Shibukawa M, et al. **Subtracted 3D CT angiography for evaluation of internal carotid artery aneurysms: comparison with conventional digital subtraction angiography.** *AJNR Am J Neuroradiol* 2006;27:1332–37 Medline
28. Kouskouras C, Charitanti A, Giavroglou C, et al. **Intracranial aneurysms: evaluation using CTA and MRA: correlation with DSA and intraoperative findings.** *Neuroradiology* 2004;46:842–50 CrossRef Medline
29. Vaphiades MS, Horton JA. **MRA or CTA, that's the question.** *Surv Ophthalmol* 2005;50:406–10 CrossRef Medline
30. Kähärä V. **Postprocedural monitoring of cerebral aneurysms.** *Acta Radiol* 2006;47:320–27 CrossRef Medline
31. Okahara M, Kiyosue H, Hori Y, et al. **Three-dimensional time-of-flight MR angiography for evaluation of intracranial aneurysms after endosaccular packing with Guglielmi detachable coils: comparison with 3D digital subtraction angiography.** *Eur Radiol* 2004;14:1162–68 Medline
32. Moody AR, Pollock JG, O'Connor AR, et al. **Lower-limb deep venous thrombosis: direct MR imaging of the thrombus.** *Radiology* 1998;209:349–55 CrossRef Medline
33. Derdeyn CP, Graves VB, Turski PA, et al. **MR angiography of saccular aneurysms after treatment with Guglielmi detachable coils: preliminary experience.** *AJNR Am J Neuroradiol* 1997;18:279–86 Medline
34. Jäger HR, Ellamushi H, Moore EA, et al. **Contrast-enhanced MR angiography of intracranial giant aneurysms.** *AJNR Am J Neuroradiol* 2000;21:1900–07 Medline
35. Evans AL, Coley SC, Wilkinson ID, et al. **First-line investigation of acute intracerebral hemorrhage using dynamic magnetic resonance angiography.** *Acta Radiol* 2005;46:625–30 CrossRef Medline
36. Thomas B, Sunaert S, Thamburaj K, et al. **Spurious absence of signal on 3D time-of-flight MR angiograms on 1 and 3 Tesla magnets in cerebral arteries associated with a giant ophthalmic segment aneurysm: the need for alternative techniques.** *JBR-BTR* 2005;88:241–44 Medline
37. Okumura A, Araki Y, Nishimura Y, et al. **The clinical utility of contrast-enhanced 3D MR angiography for cerebrovascular disease.** *Neurol Res* 2001;23:767–71 CrossRef Medline
38. Bernstein MA, Huston J 3rd, Lin C, et al. **High-resolution intracranial and cervical MRA at 3.0T: technical considerations and initial experience.** *Magn Reson Med* 2001;46:955–62 CrossRef Medline
39. McDonald RJ, McDonald JS, Kallmes DF, et al. **Intracranial gadolinium deposition after contrast-enhanced MR imaging.** *Radiology* 2015;275:772–82 CrossRef Medline
40. Zhao H, Wang J, Liu X, et al. **Assessment of carotid artery atherosclerotic disease by using three-dimensional fast black-blood MR imaging: comparison with DSA.** *Radiology* 2015;274:508–16 CrossRef Medline
41. Mehan WA Jr, Romero JM, Hirsch JA, et al. **Unruptured intracranial aneurysms conservatively followed with serial CT angiography: could morphology and growth predict rupture?** *J Neurointerv Surg* 2014;6:761–66 CrossRef Medline
42. Villablanca JP, Duckwiler GR, Jahan R, et al. **Natural history of asymptomatic unruptured cerebral aneurysms evaluated at CT angiography: growth and rupture incidence and correlation with epidemiologic risk factors.** *Radiology* 2013;269:258–65 CrossRef Medline
43. Zhu C, Sadat U, Patterson AJ, et al. **3D high-resolution contrast enhanced MRI of carotid atheroma: a technical update.** *Magn Reson Imaging* 2014;32:594–97 CrossRef Medline
44. Zhu C, Graves MJ, Yuan J, et al. **Optimization of improved motion-sensitized driven-equilibrium (iMSDE) blood suppression for carotid artery wall imaging.** *J Cardiovasc Magn Reson* 2014;16:61 CrossRef Medline
45. Viessmann O, Li L, Benjamin P, et al. **T2-weighted intracranial vessel wall imaging at 7 Tesla using a DANTE-prepared variable flip angle turbo spin echo readout (DANTE-SPACE).** *Magn Reson Med* 2017;77:655–63 CrossRef Medline
46. Naganawa S, Ito T, Shimada H, et al. **Cerebral black blood MR angiography with the interleaved multi-slab three-dimensional fast spin echo sequence.** *Radiat Med* 1997;15:385–88 Medline
47. Wang X, Zhu C, Leng Y, et al. **Intracranial aneurysm wall enhancement associated with aneurysm rupture: a systematic review and meta-analysis.** *Acad Radiol* 2018 Jun 13. [Epub ahead of print] CrossRef Medline
48. Zhu C, Tian B, Chen L, et al. **Accelerated whole brain intracranial vessel wall imaging using black blood fast spin echo with compressed sensing (CS-SPACE).** *MAGMA* 2018;31:457–67 CrossRef Medline
49. van Rooij WJ, Sprengers ME, de Gast AN, et al. **3D rotational angiography: the new gold standard in the detection of additional intracranial aneurysms.** *AJNR Am J Neuroradiol* 2008;29:976–79 CrossRef Medline
50. HaiFeng L, YongSheng X, YangQin X, et al. **Diagnostic value of 3D time-of-flight magnetic resonance angiography for detecting intracranial aneurysm: a meta-analysis.** *Neuroradiology* 2017;59:1083–92 CrossRef Medline

The authors regret that in the article "Surveillance of Unruptured Intracranial Saccular Aneurysms Using Noncontrast 3D-Black-Blood MRI: Comparison of 3D-TOF and Contrast-Enhanced MRA with 3D-DSA" (*AJNR Am J Neuroradiol* 2019;40:960–66), the legend for Fig 4 did not match the figure. A corrected legend with the original figure is reproduced below.

http://dx.doi.org/10.3174/ajnr.A6206

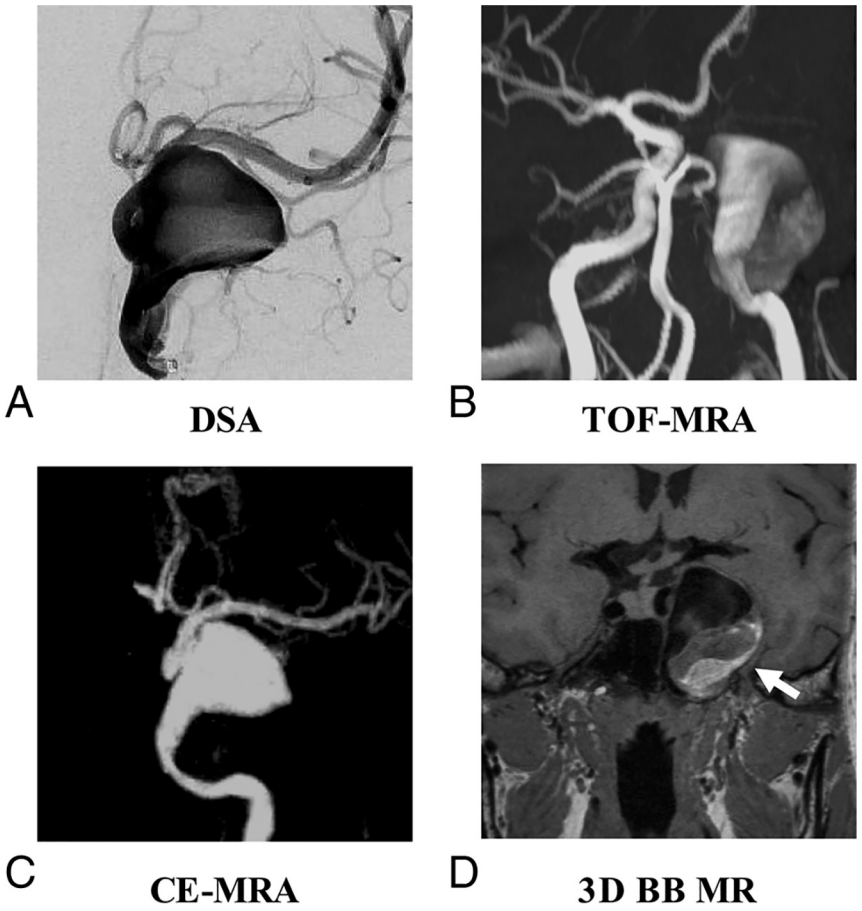

FIG 4. *A*, A 63-year-old woman with a right internal carotid artery aneurysm on DSA. 3D black-blood (BB) SPACE (*D*) can clearly visualize the sac and intraluminal thrombus of the aneurysm, which is superior to DSA (*A*), TOF-MRA (*B*), and contrast-enhanced (CE)-MRA (*C*).